SSRG International Journal of Electronics and Communication Engineering
ISSN: 2348-8549/ https://doi.org/10.14445/23488549/IJECE-V11I10P122

Volume 11 Issue 10, 266-276, October 2024

Original Article

EEG Signal-Based Emotion Detection of Parkinson's Patients for Classification and Feature Extraction by Deep Learning Architecture

Shailaja Kotte[1], J R K Kumar Dabbakuti[2]

[1,2]*Department of ECM, Koneru Lakshmaiah Education Foundation, Andhra Pradesh, India.*

[1]*Corresponding Author : shailaja.wgl@gmail.com*

Received: 22 August 2024 Revised: 23 September 2024 Accepted: 22 October 2024 Published: 30 October 2024

Abstract *- EEG-based emotion classification reflects both external and internal emotional states and has applications in the interactive brain-computer interface, patient psychological health monitoring, and entertainment consumption behaviour. This leads to more accurate, organic, and meaningful human-computer interaction—variations in experimental settings and cognitive health factors present difficulties for EEG-based emotion recognition in practical applications. The second most prevalent neurodegenerative condition, Parkinson's Disease (PD), impairs the ability to recognize and express emotions. This research proposes a novel method in EEG signal-based emotion detection of Parkinson's patients by classification and feature extraction utilizing Deep Learning (DL) methods. EEG brain waves from Parkinson's patients are used as the input, cleaned up and normalized to produce EEG fragments. Quantum convolutional learning has been used to extract features from the processed input EEG signal. Then, the extracted features are classified utilizing spatial encoder back propagation neural networks, and the classified output shows the detected emotions of Parkinson's patients. The experimental analysis is carried out for different Parkinson patient's EEG brain wave datasets regarding accuracy, precision, recall, F-1 score, SNR, RMSE and MAP.*

Keywords *- Electroencephalogram, Emotion recognition, Parkinson patients, Feature extraction, Classification.*

1. Introduction

Emotional states are linked to a wide range of human emotions, ideas, and behaviours; as a result, they impact our capacity for rational behaviour in situations involving decision-making, perception, and human intelligence. As a result, research on emotion recognition utilizing emotional signals improves the effectiveness of Brain-Computer Interface (BCI) methods for use in therapeutic settings and social interactions [1]. Emotional states are being studied in order to understand better therapies for psychological diseases such as Autism Spectrum Disorder (ASD), Attention Deficit Hyperactivity Disorder (ADHD), and anxiety disorder [2]. EEG-based emotion recognition systems have recently attracted the attention of cognitive scientists. Automated emotion processing is built on either internal, involuntary physiological responses or external, voluntary expressions. Heartbeats and Electroencephalogram (EEG) are innate to the human body and difficult to falsify or disguise, but they are physiological responses to a particular emotion. Recent research trends demonstrate the close relationship between EEG processing cognition and intrinsic emotion perception [3]. People with PD exhibit deficits in emotional prosody, diminished startle responsiveness to highly upsetting unpleasant images, and the capacity to distinguish emotions from facial expressions. Event-Related Potential (ERP) data supporting early emotional prosody processing are few. A few research concentrate on the PD perception of valence and arousal components in addition to specific emotions. Previous research demonstrates that PD patients have impaired sensitivity to highly stimulating images and impairment in recognizing positive and negative valence emotions from prosody and facial expressions. In addition to interpreting non-verbal social behaviour like emotional voice and facial expressions, the ability to recognize emotions is essential for effective social interaction and communication [4]. Unable to be purposefully suppressed, implicit physiological or bio-signals indicate the distinctive functioning of the central nervous system. Recent research has extensively used biosignals to examine how healthy participants perceive emotions.

In comparison to other modalities, EEG, MRI, MEG, and PET provide trustworthy data on emotional states. EEG is non-invasive, has a high temporal resolution, and can detect minute changes in brain activity. Emotions have been linked to specific EEG frequency bands [5]. CNNs may automatically learn cognitive and emotional correlations, whereas hand-coded EEG descriptors like Spectral Power Vectors enable emotion identification [6].

The contribution of this article is as follows:

1. To propose a novel approach in EEG signal-based emotion detection of Parkinson's patients by classification and feature extraction using deep learning techniques.
2. EEG brain waves from Parkinson's patients are collected and processed for noise removal and normalization to obtain EEG fragments.
3. The processed input EEG signal features were extracted using quantum convolutional learning.
4. Then, using spatio encoder back propagation neural networks to classify the extracted features, the output shows the emotions of Parkinson's patients that were discovered.

2. Related Works

Along with motor symptoms, PD patients also exhibit cognitive and emotional abnormalities [7]. Meanwhile, [8, 9] notice reduced recognition of disgust, indicating PD abnormalities in recognizing the facial emotions of fear and disgust. PD patients with left hemisphere disease report diminished surprise recognition and impaired anger recognition. While [10] highlights that anger and fear are less likely to be recognized, note deficiencies in perceiving sadness, rage, and disgust in PD. An initial PD deficit [11] for negative emotions and a later deficit for positive emotions are seen, according to a meta-analysis. In certain research [12], auditory and verbal cues, for example, are used to measure PD emotion deficits. Patients with Parkinson's disease generally have decreased expression and recognition in an emotive voice test [13]. Reduced recognition of fear, surprise, and disgust from text is observed and confirms this result [14]. However, several researches suggest that PD only slightly affects the ability to recognize facial expressions [15]. Earlier attempts have utilized the potential of EEG for emotion elicitation using a variety of standard feature extraction approaches [16]. In conventional methods, SVM and LDA classifiers are utilized to study FFT, STFT, DWT, statistical features, PSD, and a combination of these features [17]. The influence of a number of emotion classes evaluated by the same research is lowered from the SEED dataset's accuracy of 83.81% for 3 classes of emotion to the SEED-IV dataset's accuracy of 58.87%, a substantial accuracy drop of 24.94% [18]. Post-hoc interpretability may be a solution, which involves building a sophisticated neural model and then analyzing it [19].

Along with surrogate models, gradient-based techniques like those used in saliency maps and Locally Interpretable Model Explanations (LIME) can also create interpretability. Alternatively, machine learning models that are interpretable by design can be trained. In this vein, the SincNet new model has been put out [20-22].

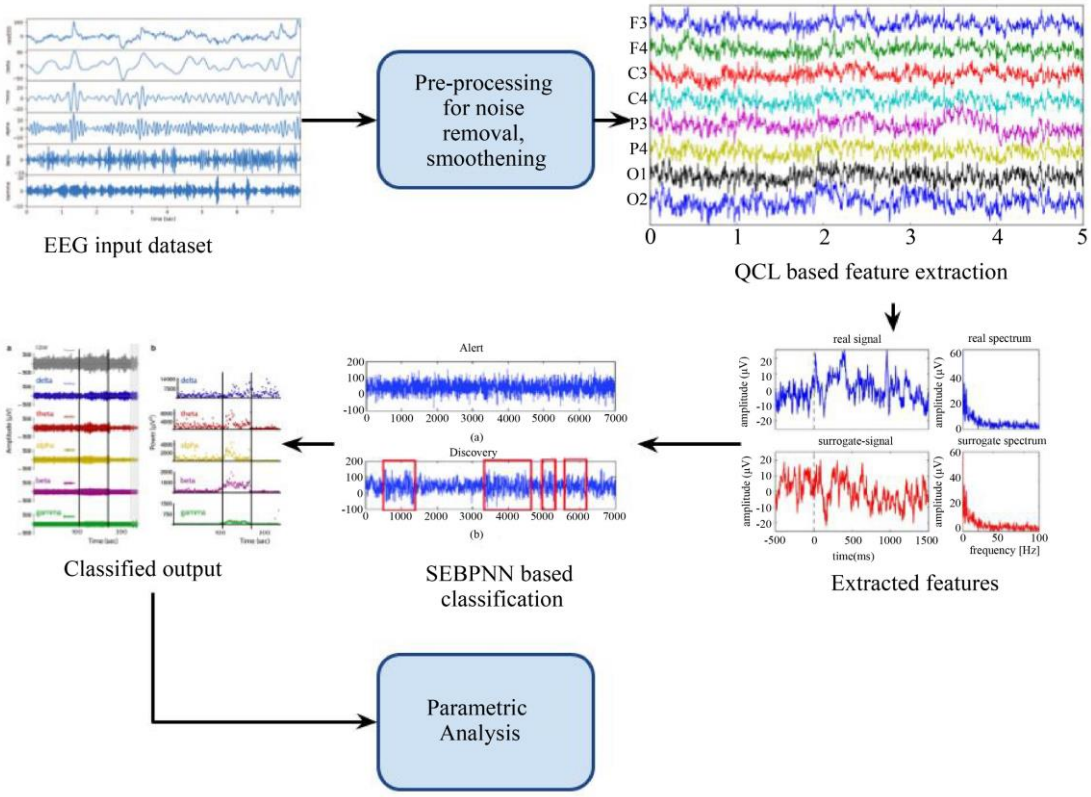

Fig. 1 The overall proposed architecture

3. Materials and Methods

3.1. The System Model

This section discusses a novel method for classifying and extracting features from EEG signals to identify Parkinson's patients' emotions. Here, the input is gathered as EEG brain waves from Parkinson's patients, which are then processed for noise removal and normalization to produce EEG fragments. Quantum convolutional learning has been used to extract features from the input EEG signal that has been processed. Then, using a spatio encoder back propagation NN to classify the extracted features, the output shows the emotions of Parkinson's patients that were discovered. In Figure 1, the suggested architecture is shown.

The recordings were made for 5 minutes at a sampling rate of 128 Hz while the subject was at rest to achieve a calm wakefulness. 14 channels of an emotive EPOC neuro headset were employed. Before the recording, the participants were instructed to find a quiet place to sit and not move their bodies (such as blinking their eyes) while it was being recorded. The signals were divided into 2-s window lengths after the recording. A threshold approach was utilized to exclude signal amplitudes greater than 100 lV to reduce eye blinking artefacts. The frequency range of 1-49 Hz was then filtered using a forward reverse filtering method with a 6th-order bandpass Butterworth filter. Finally, 1588 epochs without artefacts were analyzed for more research.

3.2 Quantum Convolutional Learning-Based Feature Extraction

In the qubit neuron model, quantum states and neuron states are connected, and operations resulting from quantum calculations are used to transfer between neuron states. A random neuron's state $|\varphi\rangle$ is determined by Equation (1),

$$|\varphi\rangle = \alpha|0\rangle + \beta|1\rangle \tag{1}$$

Where |1| and |0| are, respectively, a firing neuron and a nonfiring neuron. Additionally, $\alpha|^2$ and $|\beta|^2$ represent the likelihood that a qubit will measure 0 or 1. Consequently, we have Eqution (2),

$$|\alpha|^2 + |\beta|^2 = 1 \tag{2}$$

The inner product and the products that follow fit into the right side of the conventional model. T has two possible quantum states by Equation (3).

$$|\phi_x\rangle = \frac{1}{\sqrt{m}} \sum_{j=0}^{m-1} x_j|j\rangle$$

$$|\phi_w\rangle = \frac{1}{\sqrt{m}} \sum_{j=0}^{m-1} w_j|j\rangle \tag{3}$$

State |j is the jth weight state, and wj is the encoded weight's value in Equation (6), which is the same. The inner product is followed by Equation (4).

$$\langle \phi_x \mid \phi_w \rangle = \frac{1}{m} \sum_{j=0}^{m-1} x_j w_j \tag{4}$$

It has a parameter of $\frac{1}{m}$ Moreover, it represents the linear equation of every neuron. Starting from the quantum state |0, $\phi, \psi\rangle$ inner product of 2 quantum states is calculated. After that, use a Hadamard gate to transform the system's state into the superposition $\frac{1}{\sqrt{2}}(|0, \phi, \psi\rangle + |1, \phi, \psi\rangle)$. After that, convert the superposition into $\frac{1}{\sqrt{2}}(|0, \phi, \psi\rangle + |1, \psi, \phi\rangle)$.It implies that by reading out the outcome of the first qubit's measurement, we can obtain ||||. It is not always positive, nevertheless, for feature vector x as well as weight vector w to be combined. It implies that it is insufficient to have absolute value merely. We can calculate the likelihood of measuring the first qubit to be in state |0 using the analysis above by Equation (5):

$$P_0 = \frac{1}{2} + \frac{1}{2}|\langle x \mid w \rangle|^2 \tag{5}$$

$$\vec{x}^T \cdot \vec{w} = 2\sqrt{2P_0 - 1} \tag{6}$$

The range of this equation's x|w is [0, 1]. We should scale the appropriate portion of the equation suitably to address the issue that the inner product is always positive. In reality, dot product $\vec{x}^T \cdot \vec{w}$ is anticipated rather than the actual inner product x|w. That says it is possible to get the right answer to the neuron equation if $\vec{x}^T \cdot \vec{w}$ is derived from the entire inner product x|w. Think about Equation (7).

$$\vec{x}^T \cdot \vec{w} = 2\sqrt{2P_0 - 1} - 1 \tag{7}$$

This falls inside the range [1, 1]. The probability amplitudes are first converted from classical data into a quantum state by normalizing vectors x and w by Equation (8).

$$\left(\frac{x_0}{Z_x}, \frac{x_1}{Z_x}, \ldots, \frac{x_{m-1}}{Z_x}\right)\left(\frac{w_0}{Z_w}, \frac{w_1}{Z_w}, \ldots, \frac{w_{m-1}}{Z_w}\right) \tag{8}$$

Where Z_x is $\sqrt{x_0^2 + x_1^2 + \cdots + x_{m-1}^2}$ and Z_w is $\sqrt{w_0^2 + w_1^2 + \cdots + w_{m-1}^2}$ Obviously, it has eqn (9)

$$\left(\frac{x_0}{Z_x}\right)^2 + \left(\frac{x_1}{Z_x}\right)^2 + \cdots + \left(\frac{x_{m-1}}{Z_x}\right)^2 = 1$$

$$\left(\frac{w_0}{Z_w}\right)^2 + \left(\frac{w_1}{Z_w}\right)^2 + \cdots + \left(\frac{x_{m-1}}{Z_w}\right)^2 = 1 \tag{9}$$

The result of dividing the aforementioned equations by two on both sides is by Equation (10).

$$\frac{x_0^2}{2Z_x^2}+\frac{x_1^2}{2Z_x^2}+\cdots+\frac{x_{m-1}^2}{2Z_x^2}=\frac{1}{2}$$

$$\frac{w_0^2}{2Z_w^2}+\frac{w_1^2}{2Z_w^2}+\cdots+\frac{x_{m-1}^2}{2Z_w^2}=\frac{1}{2} \quad (10)$$

Another half needs to be added on both sides to meet the requirement that probability sum equals one by eqn (11):

$$\frac{x_1^2}{2Z_x^2}+\cdots+\frac{w_{m-1}^2}{2Z_x^2}+\frac{w_1^2}{2Z_w^2}+\cdots+\frac{1}{2}=1$$

$$\frac{w_1^2}{2Z_x^2}+\cdots+\frac{w_{m-1}^2}{2Z_x^2}+\frac{w_1^2}{2Z_w^2}+\cdots+\frac{1}{2}=1 \quad (11)$$

Equations (15) and (16) separately relate to the normalizing parameters by Equatiion (12).

$$\left(\frac{x_0}{\sqrt{2}Z_x},\frac{x_1}{\sqrt{2}Z_x},\ldots,\frac{x_{m-1}}{\sqrt{2}Z_{m-1}},\frac{1}{\sqrt{2}}\right)$$

$$\left(\frac{w_0}{\sqrt{2}Z_w},\frac{w_1}{\sqrt{2}Z_w},\ldots,\frac{w_{m-1}}{\sqrt{2}Z_{m-1}},\frac{1}{\sqrt{2}}\right) \quad (12)$$

$$P_0=\frac{1}{2}+\frac{1}{2}\left|\frac{1}{2}\langle x'\mid w'\rangle\right|^2=\frac{1}{2}+\frac{1}{2}\left|\frac{1}{2}(x_0'w_0'+x_1'w_1'+\cdots+x_{m-1}'w_{m-1}')+\frac{1}{2}\right|^2$$
$$=\frac{1}{2}+\frac{1}{2}\left|\frac{1}{2}\vec{x}'^T\vec{w}'+\frac{1}{2}\right|^2 \quad (13)$$

Now, it is possible to solve Equation (10) and use the quantum neuron. The coefficient vector is enlarged by one dimension using this technique; it should be noted. This implies that an additional qubit will be required if the dimension of the coefficient is 2n before it is normalized in order for it to store all the data of classical data. CNN layers, which lessen noise and identify certain morphological patterns, are regarded as fuzzy filters. Transformation applied by neural layers is initially parameterized by its weight, w.

$$x_i^l=f\left(\sum_j w_{ij}^l x_j^{l-1}+b_i^l\right) \quad (14)$$

The output of the convolutional layer is shown by x l I while b l I represents the bias coefficient of neuron ith in layer l, which is set in CNN layers and fully linked layers. Equation (2) is used to calculate this ReLU(x) function by Equation (15).

$$f(x)=\max(0,x_i) \quad (15)$$

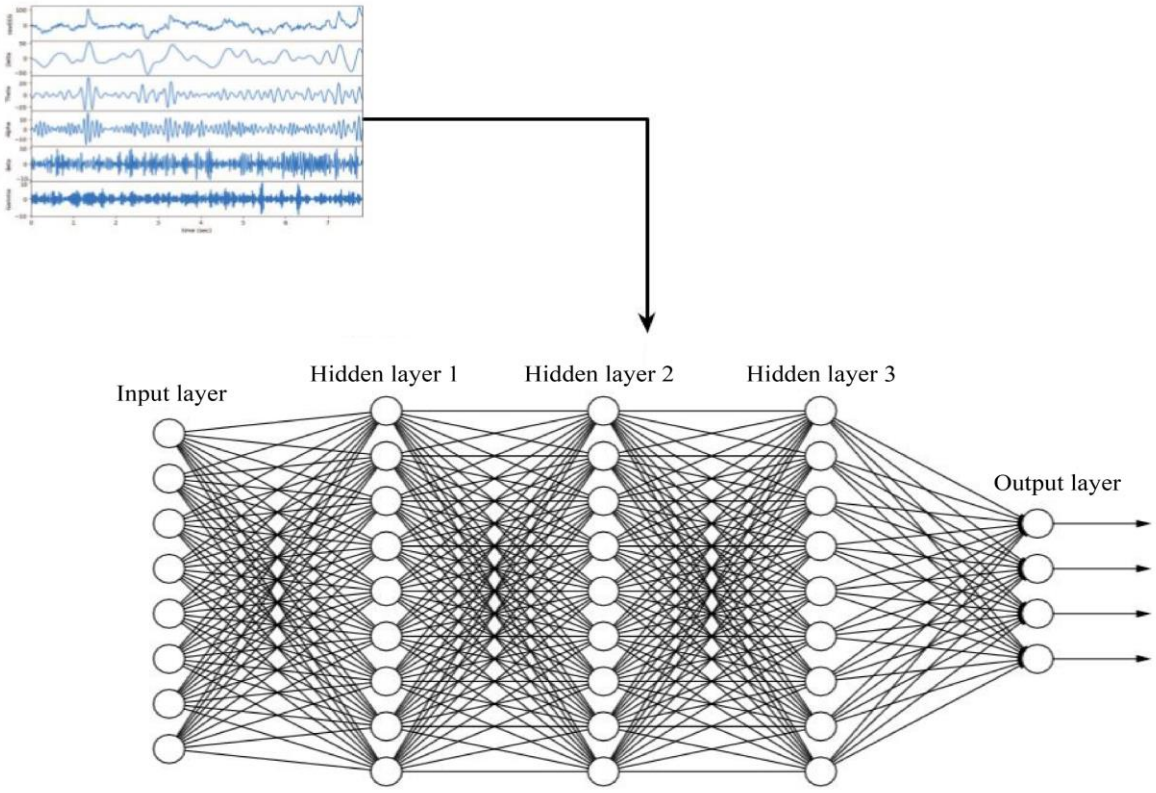

Fig. 2 Architecture of emotion recognition process using Convolutional learning

In order to segment a convolutional region that can improve the resilience of features as well as decrease the dimensionality of the physiological signals vector, the cross-entropy loss function is then established in a fully connected layer to evaluate emotion recognition, as shown in Equation (16).

$$E = \frac{1}{2}\sum_{j=1}^{N}\left(y_i - c_j\right)^2 \tag{16}$$

Figure 2 depicts the deep learning-based model for emotion recognition. Additionally, the way input vectors are transformed in local patches inside a convolution window is understood.

3.3. Spatio Encoder Back Propagation Neural Networks

The stochastic metapopulation model's system state is represented by the nsm matrix $(t) = (\boldsymbol{N}\ (k)\ i\ (t))$=1,…,$ns$,k=1,…,m, where $\boldsymbol{N}\ (k)\ i\ (t)$ is number of members. Given the total number of agents, na, the set of all potential method states is represented by Mn by Equation (17).

$$\mathbb{M}_{n_a} := \left\{N = \left(N_i^{(k)}\right)_{i=1,\ldots,n_s,k=1,\ldots,m} \in \mathbb{N}_0^{n_s,m} : \sum_{i=1}^{n_s}\sum_{k=1}^{m} N_i^{(k)} = n_a\right\} \tag{17}$$

Similar to this, an adoption event in subpopulation k from status I to status j causes a change in the system state of type $(t) \to (t) - E\ (k)\ i + E\ (k)\ j$. Let $P\ (N, t) :=$ P($\boldsymbol{N}(t) = N$)indicate the likelihood that the system will be in state $N \in$ Mna at time t. We regard Equation (7) of the ABM as an analogue to Equation (18).

$$\frac{d}{dt}P(N,t) = \mathscr{L}P(N,t) + CP(N,t)$$
$$\mathscr{L}P(M) := \sum_{N\in\mathbb{M}_{n_a}} \hat{\mathscr{L}}_{NM}\cdot P(N) \tag{18}$$

When $N = (N\ (k)\ ) \in$ Mna, the indicator ansatz functions are defined by Equation (19)

$$\Phi_N(X,S) := \prod_{k=1}^{m}\prod_{i=1}^{n_s}\phi_{N_i^{(k)}}(X,S)$$

With

$$\phi_{N_i^{(k)}}(X,S) := \delta_{N_i^{(k)}}\left(\sum_{\alpha=1}^{n_\alpha}\delta_{A_k}(x_\alpha)\delta_i(s_\alpha)\right) \tag{19}$$

Where δ stands for set-based indicator functions as well as the Kronecker delta. In other words, N (X, S) is equal to 1 when there are exactly N (k) I agents with position $x\alpha \in Ak$and status s = I and zero otherwise.

Since these ansatz functions satisfy $\sum N \in$ M$na\Phi N\ (X, S)$ = 1 for all $(X, S) \in$ Y for any $(X, S) \in$ Y and are hence non-negative, they constitute a partition of unity. The inner product of 2 functions f, g: Y → R is therefore defined as by Equation (20).

$$\langle f, g\rangle := \frac{1}{(\mu(\mathbb{X})n_s)^{n_a}}\sum_{S\in\mathbb{S}^{n_a}}\int_{\mathbb{X}^{n_a}} f(X,S)g(X,S)dX$$

$$Qv = \sum_{N\in\mathbb{M}_{n_a}} \frac{\langle\Phi_N, v\rangle}{\langle\Phi_N, \mathbb{1}\rangle}\Phi_N \tag{20}$$

Finding matrix representations $\hat{\mathscr{L}} = \left(\hat{\mathscr{L}}_{NM}\right)_{N,M\in M_{n_a}} \hat{\mathcal{G}} = \left(\hat{\mathcal{G}}_{NM}\right)_{N,M\in\mathbb{M}_{n_a}}$ of the projected operators QLQ and QGQ for operators L and G described in (5) and (6) is the objective at this point. We start by thinking about spatial dynamics. Define by Equation (21)

$$\lambda_i^{(kl)} := \frac{\left\langle\delta_{A_l}, L_i\delta_{A_k}\right\rangle_{\mathbb{X}}}{\left\langle\delta_{A_k}, \mathbb{1}\right\rangle_{\mathbb{X}}} = \frac{\int_{\mathbb{X}}\delta_{A_l}(x)\left(L_i\delta_{A_k}\right)(x)dx}{\int_{\mathbb{X}}\delta_{A_k}(x)dx} \tag{21}$$

Where 1 stands for constant 1-function on X and X is the usual scalar product for functions in L2 (X). Here, we examine first- and second-order adoptions independently as the two essential situations by Equation (22):

$$\gamma_{ij}^{(k)} := \frac{\left\langle y_{ij}, \delta_{A_k}\right\rangle_{\mathbb{X}}}{\left\langle\delta_{A_k}, \mathbb{1}\right\rangle_{\mathbb{X}}} = \frac{\int_{\mathbb{X}}\gamma_{ij}(x)\delta_{A_k}(x)dx}{\int_{\mathbb{X}}\delta_{A_k}(x)dx}$$

Where

$$\hat{f}_{ij}^{(k)}(N) := \gamma_{ij}^{(k)}N_i^{(k)}. \tag{22}$$

The spatio-temporal master equation is a form of the SMM equation provided by (23):

$$\frac{dP(N,t)}{dt} = -\sum_{\substack{k,i=1\\k\neq l}}^{m}\sum_{n_s}\lambda_i^{(kl)}N_i^{(k)}P(N,t) + \sum_{\substack{k,=1=1\\k\neq l}}^{m}\sum_{i=1}^{n_s}\lambda_i^{(kl)}\left(N_i^{(k)}+1\right)P\left(N + E_i^{(k)} - E_i^{(l)}, t\right) - \sum_{i,j=1}^{n_s}\sum_{k=1}^{m}\hat{f}_{ij}^{(k)}(N)P(N,t) + \sum_{i,j=1}^{n_s}\sum_{k=1}^{m}\hat{f}_{ij}^{(k)}\left(N + E_i^{(k)} - E_j^{(k)}\right)P\left(N + E_i^{(k)} - E_j^{(k)}, t\right) \tag{23}$$

Where the first 2 phrases on the right-hand side describe alteration brought about by subpopulation exchange. In a pathwise notation, the stochastic process $((t)) \in$T described by (24) can be represented as follows:

$$N(t) = N(0) + \sum_{\substack{k=1=1\\k\neq 1}}^{m}\sum_{i=1}^{n_s}\mathcal{R}_i^{(kl)}\left(\int_0^t\lambda_i^{(kl)}N_i^{(k)}(s)ds\right)\left(E_i^{(l)} - E_i^{(k)}\right) + \sum_{i,j=1}^{n_s}\sum_{k=1}^{m}\mathcal{P}_{ij}^{(k)}\left(\int_0^t\hat{f}_{ij}^{(k)}(N(s))ds\right)\left(E_j^{(k)} - E_i^{(k)}\right) \tag{24}$$

Where $\mathcal{P}_{ij}^{(k)}$ and $\mathscr{R}_i^{(kl)}$denote separate Poisson processes with a unit rate.

$$\hat{\mathrm{N}}(t) = \hat{\mathrm{N}}(0) + \sum_{k,l=1,k\notin l}^{m}\sum_{i=1}^{n_s}\mathcal{P}_i^{(kl)}\left(\int_0^t \lambda_i^{(kl)}\hat{N}_i^{(k)}(s)ds\right)\left(E_i^{(l)} - E_i^{(k)}\right) + \sum_{i,j=1}^{n_s}\sum_{k=1}^{m}\int_0^t f_{ij}^{(k)}(\hat{N}(s))ds\left(E_j^{(k)} - E_i^{(k)}\right) \quad (25)$$

The deterministic status-adoption dynamics for our example of two-status dynamics in a double-well potential are given by Equation (26).

$$\hat{\mathrm{N}}(t_0+\tau) = \hat{N}(t_0) + \sum_{k=1}^{m}\int_{t_0}^{t_0+\tau}\hat{f}_{12}^{(k)}(\hat{N}(s))\left(E_2^{(k)} - E_1^{(k)}\right)ds \quad (26)$$

τ<$t1 - t0$ represent time points of two consecutive stochastic transition occurrences that were brought about by the first line of (27). Following ODE is obtained for N(k) 2 of agents in subpopulation k with status 2 using the definition (19) of f(k)12:

$$\frac{d\hat{N}_2^{(k)}(t)}{dt} = \hat{\gamma}_{12}^{(k)} \cdot \hat{N}_1^{(k)}(t)\hat{N}_2^{(k)}(t) \quad (27)$$

Where $t0$ <t<$t1$. This number is constant across two transition occurrences; therefore, we may change $N`(k)$ 1 $(t)$ = $n$ $(k)$ 0 – $N`(k)$ 2 (t) in Equation (28) to get to,

$$\frac{d\hat{N}_2^{(k)}(t)}{dt} = \hat{\gamma}_{12}^{(k)}\hat{\mathrm{N}}_2^{(k)}(t)\left(n_0^{(k)} - \hat{N}_2^{(k)}(t)\right) \quad (28)$$

The logistic function provides the answer; therefore, we can solve the problem analytically by Equation (29).

$$\hat{N}_2^{(k)}(t) = n_0^{(k)}\left(1 + e^{-\hat{\gamma}_{12}^{(k)}n^{(k)}(t_0)t}\left(n_0^{(k)} - \hat{N}_2^{(k)}(t_0)\right)\right)^{-1} \quad (29)$$

For $t0$ <t<$t1$, treating diffusive transitions between subpopulations as random occurrences that cause jumps in the PDMM process's state N.

Then the function is the partial derivative of weight space (5a). Similar to that, these three changeable parameters' partial derivatives are functions by Equation (30).

$$f_A^{'} = \frac{\partial f\left(A_j, U_j, L_j, T_j\right)}{\partial A_j} = -\frac{\left(y_j - U_j\right)\left(y_j - L_j\right)}{T_j\left(U_j - L_j\right)}$$
$$f_{U_j} = \frac{\partial f\left(A_j, U_j, L_j, T_j\right)}{\partial U_j} = \frac{1}{1+e^{-A_i/J_j}} \quad (30)$$

As for the output unit, the following is the evaluation function for the error signal of A, U, L, and T by Equation (31):

$$\delta_{A_j} = f_{A_j}^{'}(di - yi)$$
$$\delta_{U_j} = f_{U_j}^{'}(dj - yj)$$
$$\delta_{L_j} = f_{L_j}^{'}(dj - yj) \quad (31)$$

The aforementioned functions, however, do not apply to the middle layer [6] since there is not an optimum output there. According to function (7a), the connecting unit's error signal and connection weights are used to calculate the middle layer unit's error signal.

Similar to how the connection unit's BP value is utilized to calculate the error signal of middle layer units U, L, and T by Equation (32).

$$\delta_{A_j} = f_{A_j}'\sum_k \delta_{A_k} w_{jk}$$
$$\delta_{U_j} = f_{U_j}'\sum_k \delta_{U_k} w_{jk}$$
$$\delta_{L_j} = f_{L_j}'\sum \delta_{L_k} w_{jk}$$
$$\delta_{Uj} = f_{U,}'\sum \delta_{U_J} w_{jL}$$
$$\delta_{U_j} = f_{Uj}\sum_k \delta_{U_k} w_{jk} \quad (32)$$

Connection weights, thresholds, U, L, and T of each unit must be modified in accordance with the estimated error signal during the BP process, as follows by Equation (33):

$$\Delta w_{ij}(n+1) = \eta_A \delta_{A_j} y_j + \alpha_A \Delta w_{ij}(n)$$
$$\Delta\theta_j(n+1) = \eta_A \delta_{A_j} + \alpha_A \Delta\theta_j(n)$$
$$\Delta U_j(n+1) = \eta_{UL} \delta_{U_j} + \alpha_{UL} \Delta U_j(n)$$
$$\Delta L_j(n+1) = \eta_{UL} \delta_{L_j} + \alpha_{UL} \Delta L_j(n)$$
$$\Delta T_j(n+1) = \eta_T \delta_{T_j} + \alpha_T \Delta T_j(n) \quad (33)$$

The enhanced BP learning algorithm will be outlined in the sections that follow. Similar to the function (8c), upper limitU can only be modified and then improved for the middle layer unit when U j δ is greater than zero. L also needs to be lowered.

The revised BP learning algorithm's step-by-step procedure is as follows:

1. Initialize the upper and lower limits, temperature, and connection weights of the network using random values of (-0.5, +0.5): DoFor each training pattern with 1 U =, 0 L =, and T = 1.
2. a set of desired output values and input values;
3. Evaluate real output j y from functions (2) and (4) for each PU j during the forward propagation stage of the pattern;
4. Evaluate the error signal from functions (5) and (6) and backpropagate to all linked middle layer units for each PU j; otherwise, if j is the middle layer unit, evaluate the error signal from functions (5) and (7);
5. For each PU j Update w,θ and T by the function (8a), (8b)and (8c)}};
6. Evaluate RMS using formula (1); then, examine errors while considering that.
7. End.

4. Results and Discussion

In this section evaluates the performance of the proposed model based on various assessment parameters and compares the same with existing methods. The proposed hybrid model requires the following hardware and software tools to evaluate the performance: 64-bit Operating System (OS), Intel(R) Core(TM) i5 processor, 8GB RAM, Windows 10, and the software tool such as Python 2.7 programming language with various python libraries NumPy, Pandas, Keras, and SciPy frameworks.

4.1. Dataset Description

In this research work, we used the SEED dataset, which is the publicly available dataset for researchers. In this work, a total of 15 participants or subjects were involved (7 males and 8 females) with an average age of 23.3 and a Standard Deviation (SD) of 2.4. The EEG dataset consists of the signals that were taken while the subjects were watching emotional video tapes. In order to compare neural patterns and notable responses across different subjects and EEG sessions, participants were asked to complete the trials for three sessions each. This dataset includes information from 45 various experiment sessions as a result. There was a week or more in between each subject's sessions.

The AMIGOS dataset uses the EEG, ECG, and GSR signals of 40 subjects to register their mood and affect, and due to the stimulation brought on by watching both short and long videos, personality.

Table 1. Analyzing the differences between the suggested and existing methods using a variety of EEG Parkinson datasets

Dataset	Techniques	Accuracy	Precision	Recall	F1_Score	SNR	RMSE	MAP
SEED	STFT	81	75	66	54	41	32	51
	SVM_LDA	85	77	68	59	43	34	53
	EEG_PP_DL	89	79	72	61	45	36	55
AMIGOS	STFT	85	81	73	63	47	39	56
	SVM_LDA	88	83	75	65	49	42	58
	EEG_PP_DL	92	85	78	71	52	44	60

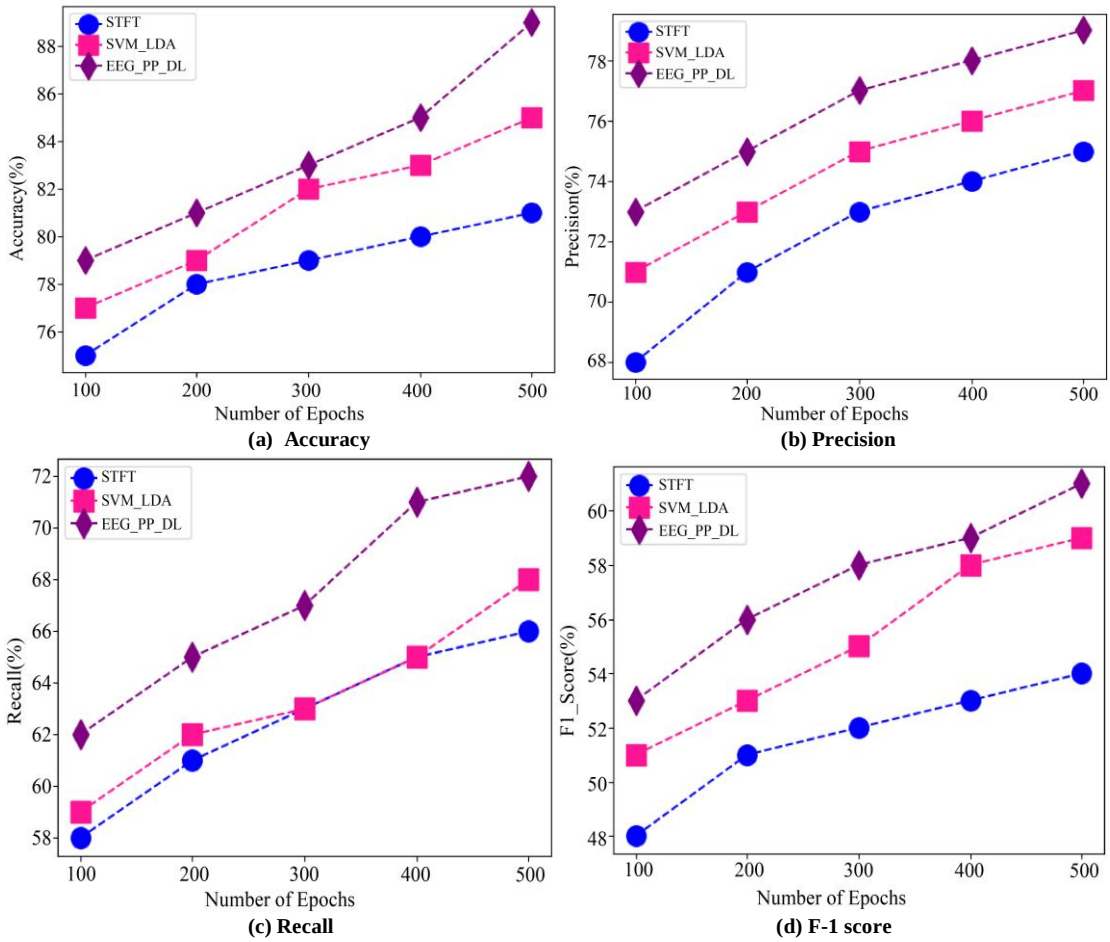

(a) Accuracy **(b) Precision**

(c) Recall **(d) F-1 score**

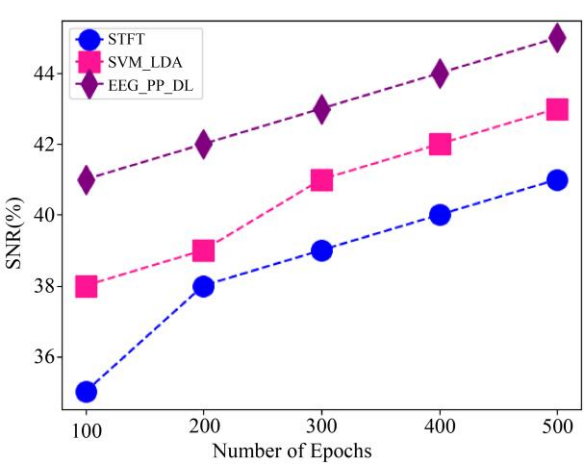

(e) SNR

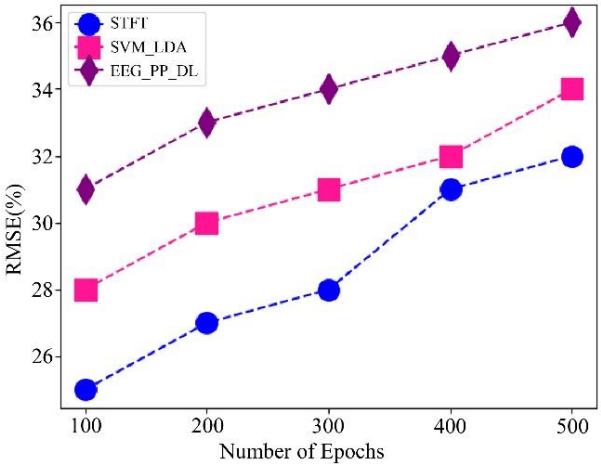

(f) RMSE

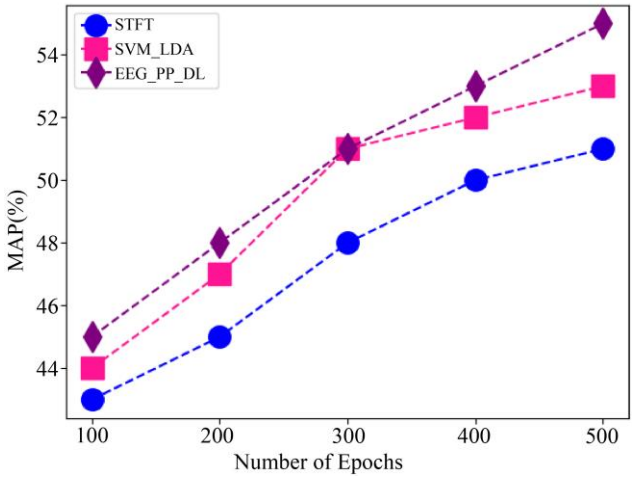

(g) MAP

Fig. 3 Parametric comparison for SEED dataset in terms of (a) Accuracy, (b) Precision, (c) Recall, (d) F-1 score, (e) SNR, (f) RMSE, and (g) MAP.

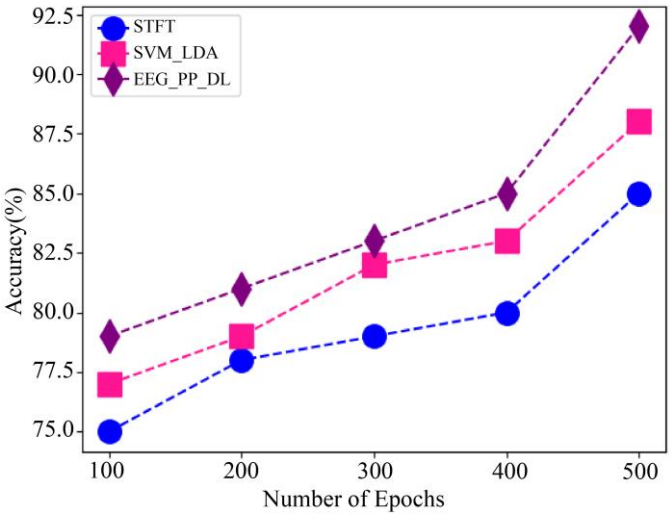

(a) Accuracy

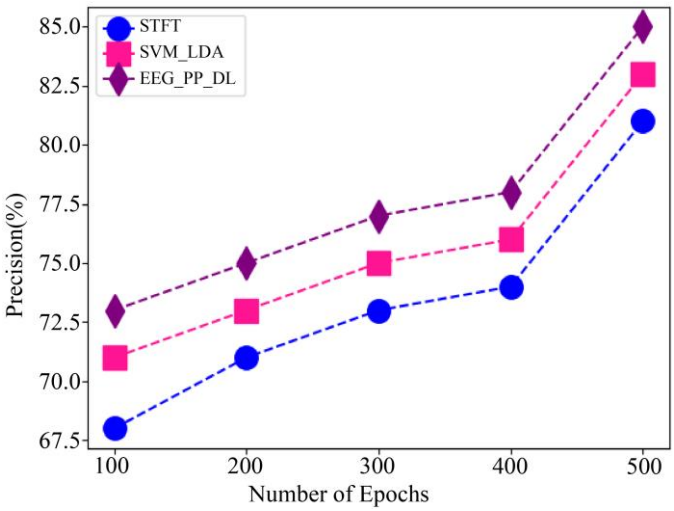

(b) Precision

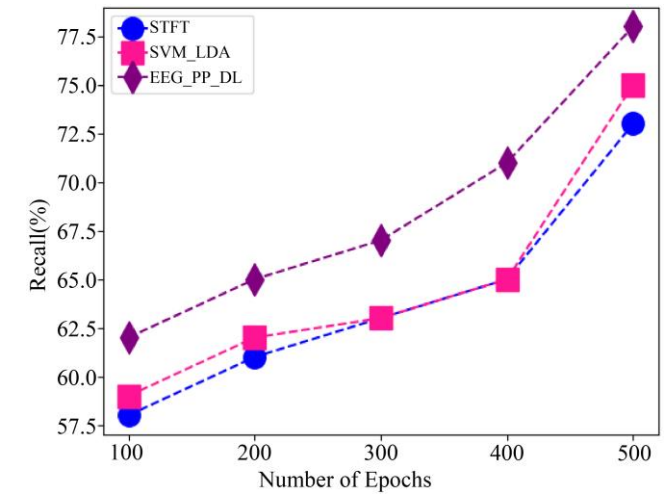

(c) Recall

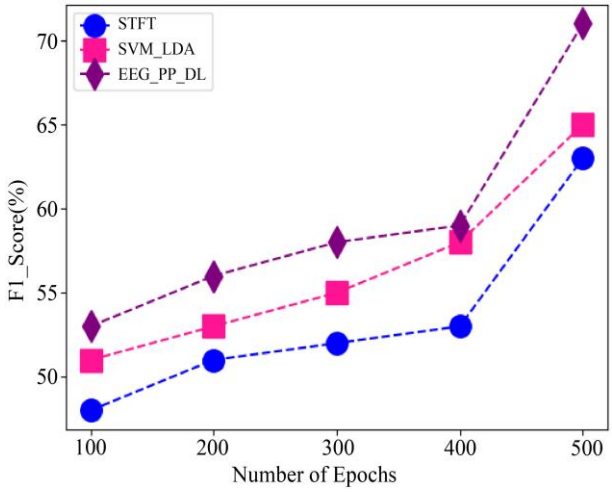

(d) F-1 score

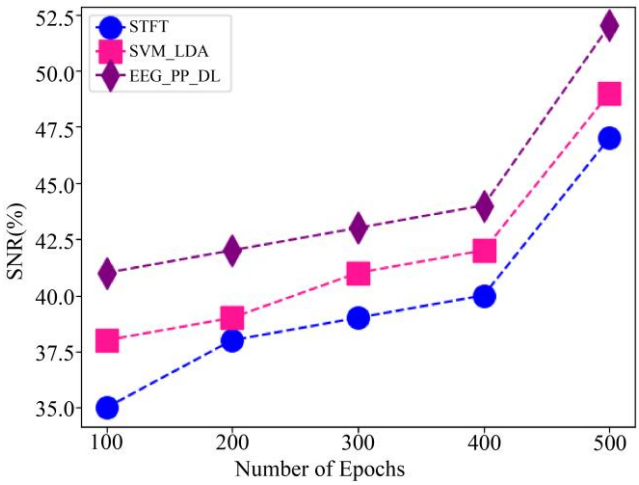

(e) SNR

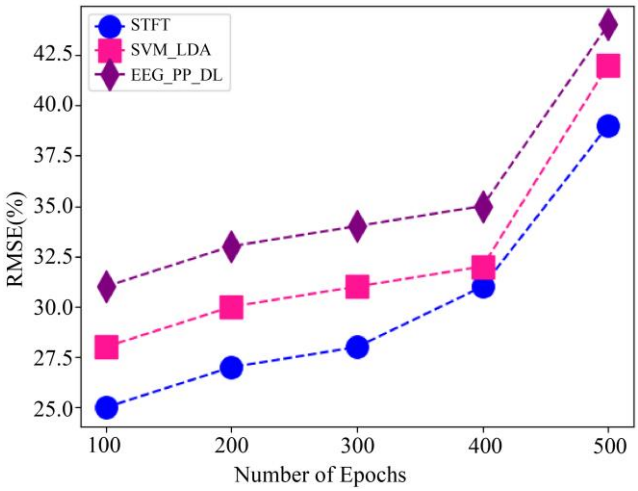

(f) RMSE

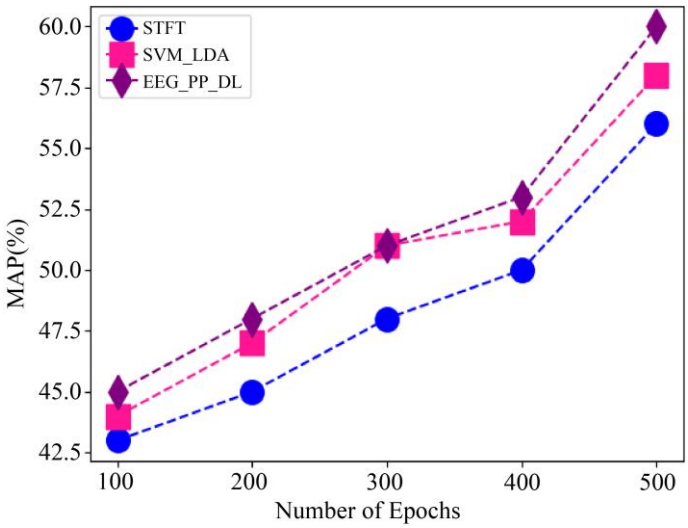

(g) MAP

Fig. 4 Parametric comparison for AMIGOS dataset in terms of (a) accuracy, (b) precision, (c) recall, (d) F-1 score, (e) SNR, (f) RMSE, and (g) MAP.

Table 1 above displays the parametric comparison of the suggested and existing techniques. Here, the accuracy, precision, recall, F-1 score, SNR, RMSE, and MAP of the AMIGOS and SEED datasets have been compared. The STFT and SVM_LDA current techniques are compared to the EEG_PP_DL suggestion. Analysis of the datasets used by both the proposed and existing techniques has been done. As shown in Figures 3(a)-(f), the proposed EEG_PP_DL achieved accuracy of 89%, precision of 79%, recall of 72%, F-1 score of 61%, SNR of 45%, RMSE of 36%, MAP of 55% for the SEED dataset, while STFT attained accuracy of 81%, precision of 75%, recall of 66%, F-1 score of 54%, SNR of 41%, RMSE of 32%, MAP of 51%. From the aforementioned AMIGOS dataset analysis, the proposed technique obtained an improved accuracy rate with precision and a low RMSE in comparison to other existing techniques and other parameters. Secondly, for the AMIGOS dataset, the proposed EEG_PP_DL achieved an accuracy of 92%, the precision of 85%, recall of 78%, F-1 score of 71%, SNR of 52%, RMSE of 44%, MAP of 60% as shown in Figures 4(a)-(f); whereas STFT attained an accuracy of 85%, precision of 81%, recall of 73%, F-1 score of 63%, SNR of 47%, RMSE of 39%, MAP of 56%, SVM_LDA obtained accuracy of 88%, precision of 83%, recall of 75%, F-1 score of 65%, SNR of 49%, RMSE of 42%, MAP of 58%. The proposed method outperformed all other techniques in terms of EEG signal extraction with classification-based emotion detection, according to the aforementioned parametric analysis. The proposed method improved the results for emotion recognition using the AMIGOS and SEED datasets, according to the analysis of the two datasets.

5. Conclusion

This research proposes a novel method in EEG signal-based emotion detection of Parkinson's patients by classification and feature extraction using deep learning techniques. The processed input EEG is recorded by nanotechnology, and the signal features have been extracted using quantum convolutional learning and classified using spatio encoder back propagation neural networks. This framework is reliable for real-time applications like psychological profile monitoring for hospitalized patients, especially those with cognitive deficits. Only one second of the EEG signal is required to elicit emotional states. In this study, the relationship between electrodes and electrode hidden layer representations with significant frequency bands is further investigated. In terms of accuracy, precision, recall, F-1 score, SNR, RMSE, and MAP, experimental analysis is done on various Parkinson patients' EEG brain wave datasets. When applied to the SEED dataset, the proposed EEG_PP_DL achieved an accuracy of 89%, precision of 79%, recall of 72%, F-1 score of 61%, SNR of 45%, RMSE of 36%, and MAP of 55%. When applied to the AMIGOS dataset, the proposed EEG_PP_DL achieved an accuracy of 92%, precision of 85%, recall of 78%, SNR of 52%, RMSE of 44%, and MAP of 60%.

Acknowledgements

This work's authors all made equal contributions.

References

[1] Ashok Vajravelu et al., "Survey and Analysis of Preprocessing OfEEG Signal," *Annals of the Romanian Society for Cell Biology*, vol. 25, no. 6, pp. 2461-2488, 2021. [Google Scholar] [Publisher Link]

[2] Pavlos Christodoulides et al., "Classification of EEG Signals From Young Adults with Dyslexia Combining a Brain Computer Interface Device and an Interactive Linguistic Software Tool," *Biomedical Signal Processing and Control*, vol. 76, 2022. [CrossRef] [Google Scholar] [Publisher Link]

[3] Yao Zhang, and Qiang Ni, "Design of Quantum Neuron Model for Quantum Neural Networks," *Quantum Engineering*, vol. 3, no. 3, 2021. [CrossRef] [Google Scholar] [Publisher Link]

[4] Stefanie Winkelmann et al., "Mathematical Modeling of Spatio-Temporal Population Dynamics and Application to Epidemic Spreading," *Mathematical Biosciences*, vol. 336, pp. 1-17, 2021. [CrossRef] [Google Scholar] [Publisher Link]

[5] Hao Pan, "An Improved Back-Propagation Neural Network Algorithm," *Applied Mechanics and Materials*, vol. 556, pp. 4586-4590, 2014. [CrossRef] [Google Scholar] [Publisher Link]

[6] Md. Asadur Rahman et al., "Emotion Recognition from EEG-Based Relative Power Spectral Topography Using Convolutional Neural Network," *Array*, vol. 11, pp. 1-11, 2021. [CrossRef] [Google Scholar] [Publisher Link]

[7] Muhammad Najam Dar et al., "EEG-Based Emotion Charting for Parkinson's Disease Patients Using Convolutional Recurrent Neural Networks and Cross Dataset Learning," *Computers in Biology and Medicine*, vol. 144, 2022. [CrossRef] [Google Scholar] [Publisher Link]

[8] Turker Tuncer, Sengul Dogan, and Abdulhamit Subasi, "A New Fractal Pattern Feature Generation Function Based Emotion Recognition Method Using EEG," *Chaos, Solitons & Fractals*, vol. 144, 2021. [CrossRef] [Google Scholar] [Publisher Link]

[9] Smith K. Khare, Varun Bajaj, and U. Rajendra Acharya, "PDCNNet: An Automatic Framework for the Detection of Parkinson's Disease Using EEG Signals," *IEEE Sensors Journal*, vol. 21, no. 15, pp. 17017-17024, 2021. [CrossRef] [Google Scholar] [Publisher Link]

[10] Abdulhamit Subasi et al., "EEG-Based Emotion Recognition Using Tunable Q Wavelet Transform and Rotation Forest Ensemble Classifier," *Biomedical Signal Processing and Control*, vol. 68, pp. 1-8, 2021. [CrossRef] [Google Scholar] [Publisher Link]

[11] Geetanjali Sharma, Abhishek Parashar, and Amit M. Joshi, "DepHNN: A Novel Hybrid Neural Network for Electroencephalogram (EEG)-Based Screening of Depression," *Biomedical Signal Processing and Control*, vol. 66, 2021. [CrossRef] [Google Scholar] [Publisher Link]

[12] Prabal Datta Barua et al., "Novel Automated PD Detection System Using Aspirin Pattern with EEG Signals," *Computers in Biology and Medicine*, vol. 137, 2021. [CrossRef] [Google Scholar] [Publisher Link]

[13] Smith K. Khare, Varun Bajaj, and U. Rajendra Acharya, "Detection of Parkinson's Disease Using Automated Tunable Q Wavelet Transform Technique with EEG signals," *Biocybernetics and Biomedical Engineering*, vol. 41, no. 2, pp. 679-689, 2021. [CrossRef] [Google Scholar] [Publisher Link]

[14] Ravikiran Parameshwara et al., "Automated Parkinson's Disease Detection and Affective Analysis from Emotional EEG Signals," *Arxiv*, pp. 1-12, 2022. [CrossRef] [Google Scholar] [Publisher Link]

[15] Ana M. Maitin, Juan Pablo Romero Muñoz, and Álvaro José García-Tejedor, "Survey of Machine Learning Techniques in the Analysis of EEG Signals for Parkinson's Disease: A Systematic Review," *Applied Sciences*, vol. 12, no. 14, pp. 1-33, 2022. [CrossRef] [Google Scholar] [Publisher Link]

[16] Sharaban Tahura et al., "Anomaly Detection in Electroencephalography Signal Using Deep Learning Model," *Proceedings of International Conference on Trends in Computational and Cognitive Engineering*, pp. 205-217, 2020. [CrossRef] [Google Scholar] [Publisher Link]

[17] Ghita Amrani et al., "EEG Signal Analysis Using Deep Learning: A Systematic Literature Review," *2021 Fifth International Conference on Intelligent Computing in Data Sciences*, Fez, Morocco, pp. 1-8, 2021. [CrossRef] [Google Scholar] [Publisher Link]

[18] Seyed Alireza Khoshnevis, and Ravi Sankar, "Diagnosis of Parkinson's Disease Using Higher Order Statistical Analysis of Alpha and Beta Rhythms," *Biomedical Signal Processing and Control*, vol. 77, 2022. [CrossRef] [Google Scholar] [Publisher Link]

[19] M. Murugappan et al., *Electroencephalogram Signals Based Emotion Classification in Parkinson's Disease Using Recurrence Quantification Analysis and Non-Linear Classifiers*, 1st ed., Computer-aided Design and Diagnosis Methods for Biomedical Applications, CRC Press, pp. 1-34, 2021. [Google Scholar] [Publisher Link]

[20] Ling Wang et al., "Multidimensional Emotion Recognition Based on Semantic Analysis of Biomedical EEG Signal for Knowledge Discovery in Psychological Healthcare," *Applied Sciences*, vol. 11, no. 3, pp. 1-19, 2021. [CrossRef] [Google Scholar] [Publisher Link]

[21] Miguel Ángel Luján et al., "A Survey on EEG Signal Processing Techniques and Machine Learning: Applications to the Neurofeedback of Autobiographical Memory Deficits in Schizophrenia," *Electronics*, vol. 10, no. 23, pp. 1-19, 2021. [CrossRef] [Google Scholar] [Publisher Link]

[22] Didar Dadebayev, Wei Wei Goh, and Ee Xion Tan, "EEG-Based Emotion Recognition: Review of Commercial EEG Devices and Machine Learning Techniques," *Journal of King Saud University-Computer and Information Sciences*, vol. 34, no. 7, pp. 4385-4401, 2022. [CrossRef] [Google Scholar] [Publisher Link]